Influence of blood vessels on the measurement of hemoglobin oxygenation as determined by time-resolved reflectance spectroscopy

H. Liu and B. Chance
University of Pennsylvania, Department of Biochemistry and Biophysics, Philadelphia, Pennsylvania 19104-6089

A. H. Hielscher[a] and S. L. Jacques
Laser Biology Research Laboratory, The University of Texas, M. D. Anderson Cancer Center, Houston, Texas 77030

F. K. Tittel
Rice University, Department of Electrical and Computer Engineering, Houston, Texas 77251-1892

(Received 30 December 1994; accepted for publication 9 May 1995)

We report the development of a heterogeneous resin-tube model to study the influence of blood vessels on the apparent absorption of the system, μ_a(sys), using a time-resolved technique. The experimental results show that μ_a(sys) depends on the absorption inside the tubes, μ_a(tube), tube diameters, and tube-to-sample volume ratios. A mathematical expression relating μ_a(sys) and μ_a(tube) is derived based on the experimental results and is verified by time-resolved Monte Carlo simulations for heterogeneous models. This analytical formula predicts that the apparent absorption coefficient measured on a biological organ is a volume-weighted sum of the absorption coefficients of different absorbing components. We present some apparent absorption coefficients measured *in vivo* in animals and humans and discuss improved algorithms that calculate the hemoglobin saturation by including background-tissue absorption and blood vessel distribution.

Key words: time-resolved reflectance, hemoglobin absorption, blood oxygenation, heterogeneity, blood vessels, Monte Carlo simulations

I. INTRODUCTION

In recent years, near-infrared reflectance measurements have been used to determine the blood oxygenation status of living biological tissues by using continuous light or time- or frequency-domain techniques.[1-8] All these methods rely on the fact that in the wavelength range of 700–900 nm oxygenated and deoxygenated hemoglobin are the major absorbers in tissues, and have very distinct absorption spectra.[9,10] Measuring light absorption in the tissue of at least two wavelengths allows us to calculate blood oxygenation and concentrations of oxygenated and deoxygenated hemoglobin.[11-15]

These techniques all assume that the absorbers are homogeneously distributed in the tissue. So far, little attention has been paid to the fact that the high-absorbing blood is actually located in vessels that are surrounded by rather low-absorbing background tissue. This is so, particularly in the case of the brain, in which the determination of hemoglobin oxygenation status is of special interest. Reflectance measurements on the outside of the head only yield an apparent absorption coefficient of a mixed tissue–blood system. Using this apparent absorption coefficient, rather than the blood absorption coefficient in algorithms to determine the blood oxygenation of the brain may yield doubtful results.

The goal of our study is to investigate the dependence of the apparent absorption coefficient on the blood absorption in blood vessels by using a time-resolved reflectance technique. We developed a resin-tube model to simulate blood vessels embedded in a background tissue. In this paper, we use the expressions μ_a(back) and μ_s'(back) and the expressions μ_a(tube) and μ_s'(tube) to represent the absorption and reduced scattering coefficients of the resin background and the absorbing turbid solution filled in the tubes, respectively. We use μ_a(sys) to note the apparent absorption coefficient of the system. Based on the experimental data obtained from the tissue phantom, an analytical expression is derived, relating the apparent absorption coefficient to the distribution and sizes of the tubes (i.e., blood vessels). The analytical expression is also verified by time-resolved Monte Carlo simulations of cylindrical blood vessels distributed in a background medium. Finally, we propose algorithms to calculate the blood saturation by including background-tissue absorption and blood vessel distribution.

II. MATERIALS AND METHODS

The experimental model was made of polyester resin (Swanson; Deep Flex Plastic Molds, Inc., Murfreesboro, TN), which is liquid and can be cast in any shape before a chemical hardener is added.[16] We mixed 0.75 mg/ml of Titanium dioxide (TiO_2) powder (Sigma Chemical Co.) with clear resin liquid to introduce scatterers, giving rise to μ_s'(back)=6 cm^{-1}. The TiO_2 powder was well dissolved in alcohol by sonicating the powder–alcohol mixture and was then added to the resin before the resin solution was hardened. The intrinsic absorption coefficient of resin is low and similar to that of blood-free tissues in the near-infrared range [μ_a(tissue)=0.02–0.04 cm^{-1}]. To make various resin-tube models, we placed different numbers of metal rods of different sizes vertically in 15 cm diam cylindrical containers and cast the resin with the rods. When the resin was almost hardened, we removed the rods, leaving hollow tubes in the resin

 0094-2405/95/22(8)/1209/9/$6.00

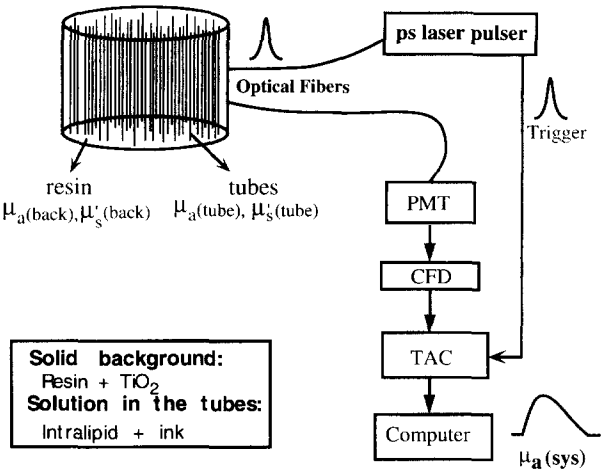

FIG. 1. A schematic diagram showing the experimental model and setup. The experimental model is made of plastic resin and mixed with a certain concentration of TiO_2. A series of vertical tubes were made through the sample and filled with an Intralipid-ink solution. 50 ps, 780 nm pulses were delivered by a 200 μm fiber to the sample, and the response signal was collected by a 2.5 mm fiber bundle and sent to a single-photon counting system. It contains a microchannel plate. Photo Multiplier Tube (PMT), a Constant Fraction Discriminator (CFD), a Time-to-Amplitude Converter (TAC), and a computer.

to simulate blood vessels of different diameters (1.6, 3.2, and 6.4 mm) that took up various volume fractions of the sample (5.5%, 11%, and 22%, respectively).

During the measurements, the tubes were filled with Intralipid-india ink solutions. An Intralipid concentration of 0.3%–1.5% was chosen to yield a reduced scattering coefficient of $\mu_s'(\text{tube})=3-15\ \text{cm}^{-1}$ for the filling solution in the tubes. The india ink concentration was varied to yield an absorption coefficient in the range of $0-5\ \text{cm}^{-1}$, which covers the range of absorption coefficients of the whole blood in the near-infrared spectrum.

As shown in Fig. 1, time-resolved reflectance measurements were performed on these samples using the method of time correlated single photon counting.[17] A Hamamatsu picosecond laser pulser at 780 nm with a pulse width of 50 ps was used. A detailed description of the detection scheme can be found elsewhere.[18] The source and detector were placed 2–3 cm apart on the side of the sample in a line perpendicular to the tubes. Once a measurement on a sample was made, the raw data were deconvolved with a separately recorded instrument function. Then a least-squares-fitting algorithm based on diffusion theory for a semi-infinite medium with a zero-boundary condition was applied to obtain the apparent absorption coefficient $\mu_a(\text{sys})$ of the sample.[19,20] Besides the measurements on the resin-tube models, measurements were also performed on homogeneous resin samples and Intralipid-ink solutions to determine the optical properties of the resin background, $\mu_a(\text{back})$, and $\mu_s'(\text{back})$, and those of the solutions filled in the tubes, $\mu_a(\text{tube})$ and $\mu_s'(\text{tube})$.

In the case of *in vivo* measurements of human heads, the source and detector of the TRS system were placed at a separation of 3 cm tightly against the right side of the forehead of five normal adult volunteers. The measurements were performed with the subjects setting down comfortably and breathing room air. In the case of *in vivo* measurements of animal heads, the source–detector separation was kept 3 cm, and the fibers were placed about 1 cm lateral to the sagittal suture over the frontoparietal cerebrum. To obtain blood-free conditions, the animals were euthanized with intravenous pentobarbital, phlebotomized, and perfused with saline until no hemoglobin was detected in the vasculature by a co-oximetry.[21] The rat liver was removed from a male rat weighing 250–300 g and perfused by Krebs–Ringer buffer solution until the output fluid became blood-free. The μ_a values of the blood-free rat liver were obtained by employing the matching method, as described in Ref. 18. The absorption of the blood-containing liver is very high so that the μ_a value was estimated by extrapolation from the absorption of the blood-free liver and the red blood cells.[22]

The signal-to-noise ratio of the single photon counting system improves in proportion to the square root of sampling time.[23] Thus, the data acquisition of each single measurement was maintained until a good signal-to-noise ratio of 200 was obtained. In this way, a singular time-response profile can give rise to an accurate singular set of μ_a and μ_s'. On the other hand, multiple measurements were also repeated to determine the accuracy of the results, and a precision of $5\pm1\%$ for the apparent μ_a and μ_s' values was obtained in most cases.

III. EXPERIMENTAL RESULTS

Two groups of resin-tube samples were studied in order to investigate the influence of vessel distribution and sizes on the apparent absorption coefficient $\mu_a(\text{sys})$. To study the influence of vessel distribution, we prepared three models having tube-to-sample volume ratios of 5.5%, 11%, and 22% while keeping the tube diameter constant. To study the influence of size, we used the models in which the tube-to-sample volume ratio was kept constant while the diameters of the tubes were changed in different models. In all these cases, only the absorption coefficient in the tubes, $\mu_a(\text{tube})$, was changed, whereas the scattering coefficient of the solution in the tubes matched that of the resin background. In addition, a study on the $\mu_a(\text{sys})$ dependence on $\mu_s'(\text{tube})$ was performed while the $\mu_a(\text{tube})$ was held constant.

A. Influence of vessel distribution

Figure 2 displays a comparison of three samples having tube-to-sample volume ratios of 5.5%, 11%, and 22%, respectively, while tube diameters are 3.2 mm in all cases. It can be seen that for small $\mu_a(\text{tube})$ values, the apparent absorption coefficient $\mu_a(\text{sys})$ depends linearly on $\mu_a(\text{tube})$ for all volume ratios. The straight lines in this figure represent a linear least-squares fit to data points with $\mu_a(\text{tube})\leq 1.5\ \text{cm}^{-1}$. When $\mu_a(\text{tube})$ becomes larger than $1.5\ \text{cm}^{-1}$, this linear relationship breaks down, and an increase in the $\mu_a(\text{tube})$ beyond $5.0\ \text{cm}^{-1}$ leads to only a negligible increase in $\mu_a(\text{sys})$. Notice that the deviation from the linear dependence starts at about the same $\mu_a(\text{tube})$ value, $1.5\ \text{cm}^{-1}$, for all three volume ratios. The ratios of the slopes of the linear-fitting lines of the volume ratio of 22% to 11% and of 22% to 5.5% are 2 and 4.5, respectively. This indicates that in the

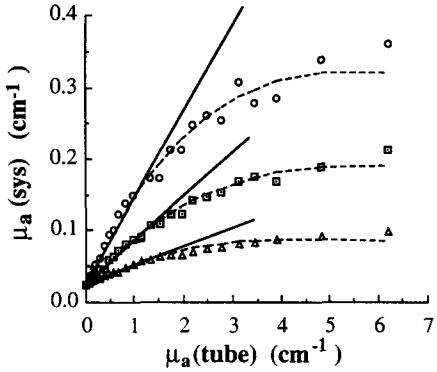

FIG. 2. The relationship between the apparent absorption coefficient of the system, μ_a(sys), and the absorption coefficient of the filling fluid in the tubes, μ_a(tube), for three samples. The samples have the same tube diameters (3.2 mm), but different tube-to-sample volume ratios of 22% (circles), 11% (squares), and 5.5% (triangles). The straight solid lines are linear least-squares fits to the data when the μ_a(tube) value is less than 1.5 cm^{-1}. The dashed curves are calculated using Eq. (7).

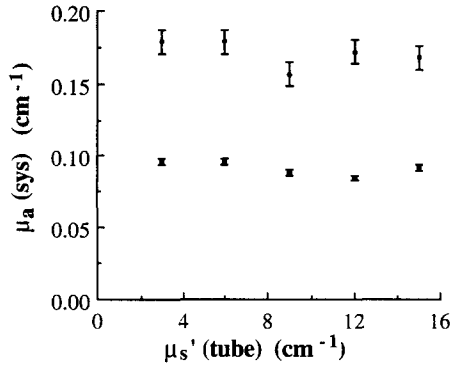

FIG. 4. The relationship between the apparent absorption coefficient of the system, μ_a(sys), and the scattering coefficient of the filling fluid in the tubes, μ_s'(tube), for a model having 3.2 mm tube diameters and a 22% tube-to-sample volume ratio at two different, fixed ink concentrations in the filling fluid. The data with smaller error bars are obtained with μ_a(tube)=0.42 cm^{-1}, and the data with larger error bars are obtained under μ_a(tube)=1.5 cm^{-1}.

linear range a doubling of the tube-to-sample volume ratio leads to a doubling of apparent absorption. Figure 2 also illustrates that doubling the volume ratio results in a doubling of the apparent absorption coefficient in the nonlinear range.

B. Influence of vessel size

Figure 3 shows the relationship between μ_a(sys) and μ_a(tube) for two samples with the same tube-to-sample volume ratio (5.5%), but with different vessel diameters (1.6 and 3.2 mm). Similar to that in Fig. 2, we can observe a linear relationship between μ_a(tube) and μ_a(sys) when μ_a(tube) values are low, whereas at higher μ_a(tube) values the apparent absorption does not follow the straight line. Furthermore, this graph shows that a sample with smaller tube diameters has a larger linear range, resulting in larger values of μ_a(sys) at μ_a(tube)>2 cm^{-1} than does a sample with larger tube diameters.

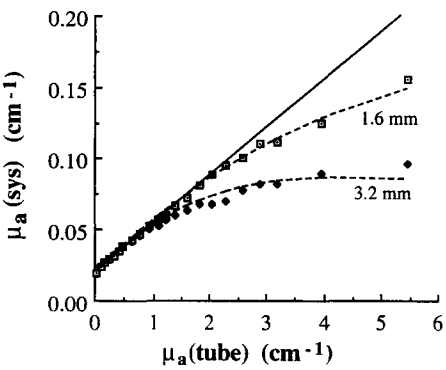

FIG. 3. The relationship between the apparent absorption coefficient of the system, μ_a(sys), and the absorption coefficient of the filling fluid in the tubes, μ_a(tube), for two samples, with 1.6 mm (open squares) and 3.2 mm (solid diamonds) tube diameters at a tube-to-sample volume ratio of 5.5%. The straight solid line is a linear least-squares fit to the 1.6 mm sample when the μ_a(tube) value is less than 1.5 cm^{-1}. The dashed curves in both figures are calculated using Eq. (7).

C. Influence of different scattering coefficients

All of the data given in Secs. III A and III B were obtained under the condition of μ_s'(back)=μ_s'(tube)=6 cm^{-1}. However, it is known that blood in vessels can have a different scattering property from that of surrounding tissue. To understand the effect of various scattering coefficients on the determination of the apparent absorption, another set of measurements was performed. In this case, we varied the scattering coefficients inside the tubes, μ_s'(tubes), by increasing the concentration of Intralipid while maintaining the μ_a(tube) constant. As an example, Fig. 4 displays the results obtained on a sample with tube diameters of 3.2 mm and a tube-to-sample volume ratio of 22%. Data shown in this figure are for two different, fixed absorption coefficients in the tubes of μ_a(tube)=1.5 cm^{-1} and μ_a(tube)=0.42 cm^{-1}. It can be seen that in the range of observation, the influence of μ_s'(tube) on μ_a(sys) can be neglected.

IV. DATA ANALYSIS

In this section, we wish to establish an analytical expression that relates the apparent absorption coefficient, μ_a(sys), to both the background absorption, μ_a(back), and the absorption in the tubes, μ_a(tube). Such a relationship will help to determine the blood absorption and thus the blood oxygenation based on apparent absorption coefficients measured on a tissue–blood system.

In a two-component system, such as the resin-tube model, we propose that μ_a(sys) is proportional to a weighted sum of component absorption coefficients:

$$\mu_a(\text{sys}) = P_b \mu_a(\text{back}) + P_t \mu_a(\text{tube}). \quad (1)$$

Weighting factors P_b and P_t are the probabilities that a detected photon has traveled either in the background or in the tubes, respectively. Because all detected photons travel through either or both of the materials, it is reasonable to have

$$P_b + P_t = 1. \quad (2)$$

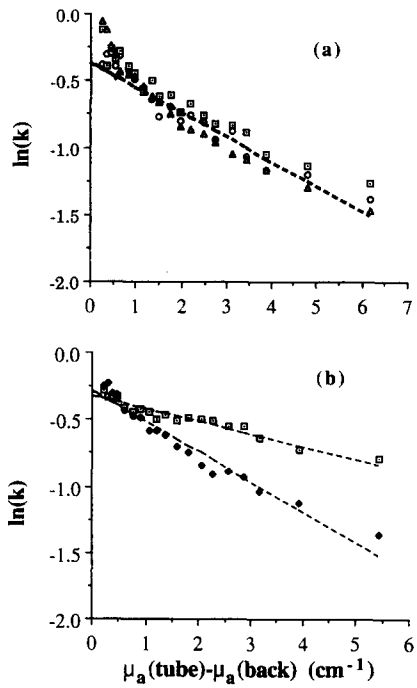

FIG. 5. Relationship between $\ln(k)$ and $[\mu_a(\text{tube})-\mu_a(\text{back})]$ for two sets of samples. (a) is for three samples with the same tube diameters (3.2 mm), but having tube-to-sample volume ratios of 22% (circles), 11% (squares), and 5.5% (triangles). The dashed line is an average of three linear fits to the three sets of data. (b) is for two samples at the same tube-to-sample volume ratio (5.5%), but with 1.6 mm (open squares) and 3.2 mm (solid diamonds) tube diameters. The dashed lines in (b) are linear least-squares fits to the data points.

The greater the number of tubes packes into a tissue, the more likely a photon will have to travel through the tubes before it reaches the detector. Thus, we further assume that P_t depends linearly on the tube-to-sample volume ratio, r_t, written as

$$P_t = k r_t. \tag{3}$$

By substituting Eqs. (3) and (2) into (1), we get

$$\mu_a(\text{sys}) = \mu_a(\text{back}) + r_t k[\mu_a(\text{tube}) - \mu_a(\text{back})], \tag{4}$$

where k is a parameter and can be rewritten as

$$k = \frac{\mu_a(\text{sys}) - \mu_a(\text{back})}{\mu_a(\text{tube}) - \mu_a(\text{back})} \frac{1}{r_t}. \tag{5}$$

All parameters on the right side of Eq. (5) can be known: r_t and μ_a(back) are given through the design of the tissue phantom, whereas μ_a(sys) and μ_a(tube) are determined through measurements. Thus, the key in finding a mathematical expression for μ_a(sys) entails obtaining parameter k, which is experimentally determinable. Based on the data given in Figs. 2 and 3, we can calculate $\ln(k)$ as a function of $[\mu_a(\text{tube})-\mu_a(\text{back})]$, as shown in Figs. 5(a) and 5(b). Figure 5(a) corresponds to three models having constant tube diameters (3.2 mm) but different tube-to-sample volume ratios. Figure 5(b) results from two samples with a constant tube-to-sample volume ratio (5.5%) but different tube diameters. These two graphs suggest that when

TABLE I. List of sample physical and mathematical parameters used for determining apparent absorption of the model. d represents the tube diameter in cm, r_t is the tube-to-sample volume ratio in percent, m is the slope of $\ln(k)$ vs $\mu_a(\text{tube})-\mu_a(\text{back})$, b is the intercept of $\ln(k)$ vs $\mu_a(\text{tube})-\mu_a(\text{back})$, α is equal to m/d, and β is equal to $\exp(-b)$.

Model #	d [cm]	r_t [%]	m	b	α	β
1	0.16	5.5	0.096	0.325	0.60	0.72
2	0.32	5.5	0.225	0.284	0.70	0.75
3	0.32	11	0.175	0.294	0.55	0.75
4	0.32	22	0.181	0.288	0.57	0.75
5	0.64	20	0.268	0.350	0.42	0.71

$[\mu_a(\text{tube})-\mu_a(\text{back})]$ is greater than 0.5 cm^{-1}, the relationship between $\ln(k)$ and $[\mu_a(\text{tube})-\mu_a(\text{back})]$ can be considered linear. Thus, we can have

$$\ln(k) = -m[\mu_a(\text{tube}) - \mu_a(\text{back})] - b, \tag{6}$$

where "m" and "b" are magnitudes of the slope and intercept of the fitting lines to the data of $\ln(k)$ vs $[\mu_a(\text{tube})-\mu_a(\text{back})]>0.5$ cm^{-1}. The fitting lines are represented by the dashed lines in Figs. 5(a) and 5(b). Replacing Eq. (6) in Eq. (4) leads to μ_a(sys) as

$$\mu_a(\text{sys}) = \mu_a(\text{back}) + r_t \beta e^{-m[\mu_a(\text{tube})-\mu_a(\text{back})]}[\mu_a(\text{tube}) - \mu_a(\text{back})], \tag{7}$$

where $\beta=\exp(-b)$. Thus, Eq. (7) is the desired mathematical expression for μ_a(sys), giving the dependence of μ_a(sys) on both μ_a(tube) and μ_a(back). This equation can, in turn, fit the data well, as shown by the dashed lines in Figs. 2 and 3, after we obtained the slope and intercept of $\ln(k)$ vs $[\mu_a(\text{tube})-\mu_a(\text{back})]$ from the experimental results.

In order to employ Eq. (7) practically, it is necessary to understand variables "m" and "b." It is seen that the slope, $-m$, is independent of tube-to-sample volume ratios [Fig. 5(a)] but dependent on tube diameters [Fig. 5(b)]. So we suggest that the value of the slope, m, may be related linearly to the tube diameter "d" by

$$m = \alpha d, \tag{8}$$

where α is a constant. Table I lists tube diameter "d," tube-to-sample volume ratio "r_t," values of slope "m," intercept "b," and parameters α and β for five different resin-tube samples. It is seen that α varies between 0.4 and 0.7, while β seems to be the same for all the samples. A constant of β indicates that β may depend mainly on the materials made for the tissue phantom. It is known that the polyester resin with added TiO_2 powder has a refractive index of 1.55 and a g value of 0.5.[16] On the other hand, Intralipid solutions have a refractive index of 1.38 and a g value of 0.7–0.9. Mismatches of refractive indices and g values between the resin background and Intralipid solution in the tubes may cause this β value. In biological tissues, β should be close to 1 since tissue background and blood in vessels have about the same refractive index and g value.

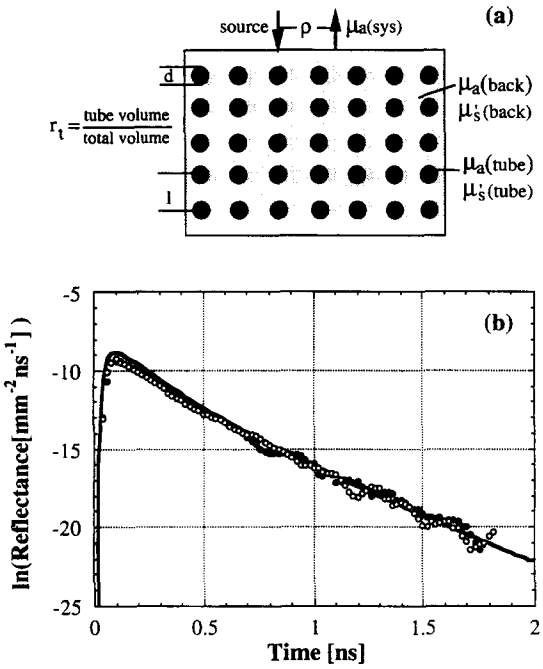

FIG. 6. Time-resolved Monte Carlo simulation results for a resin-tube model, schematically shown in (a). The input parameters are μ_a(back)=0.05 cm^{-1}, μ_s'(back)=10 cm^{-1}, μ_a(tube)=0.5 cm^{-1}, d=0.4 cm, r_t=34.9%, and ρ=1.8 cm. In (b), the empty and solid circles correspond to μ_s'(tube)=10 cm^{-1} and μ_s'(tube)=5 cm^{-1}, respectively. The solid line is calculated based on the diffusion theory with parameters of μ_a(sys)=0.194 cm^{-1} and μ_s'(sys)=10 cm^{-1}.

V. MONTE CARLO SIMULATIONS

To confirm our experimental findings of Eq. (7), we made time-resolved Monte Carlo simulations for semi-infinite, heterogeneous, resin-tube models [Fig. 6(a)] by modifying a well-tested Monte Carlo simulation code.[24] Input parameters for the simulation are the tube diameter, d, the tube-to-sample volume ratio, r_t, and optical properties of the background and the filling material in the tubes, namely, μ_a(back), μ_s'(back), μ_a(tube), and μ_s'(tube).

Circular points in Fig. 6(b) are two sets of simulated results, with d=4 mm, ρ=1.8 cm, r_t=34.9%, μ_a(back)=0.05 cm^{-1}, μ_a(tube)=0.5 cm^{-1}, and μ_s'(back)=10 cm^{-1}. The empty and solid circles correspond to μ_s'(tube)=10 cm^{-1} and μ_s'(tube)=5 cm^{-1}, respectively. The apparent reflectance signal for the system is insensitive to a doubling of μ_s'(tube) inside the tubes, consistent with the experimental result shown in Fig. 4. By substituting some of the parameters listed above into Eq. (7), we have μ_a(sys)=0.194 cm^{-1}, using α=0.5 and β=1. With this μ_a(sys) value and μ_s'(sys)=10 cm^{-1}, diffusion theory gives rise to the solid curve plotted in Fig. 6(b). We can see that the solid curve matches the simulation data well.

A variety of conditions for tube diameters, tube-to-sample volume ratios, and μ_a(tube) values have been applied to the simulations. By fitting the diffusion equation to the time-resolved simulation data, we obtain the fitted apparent absorption and scattering coefficient, μ_a(fit) and μ_s'(fit). Table II shows a comparison of absorption coefficients obtained from the Monte Carlo simulations and from Eq. (7) for the resin-tube model. In this table, d, r_t, and μ_a(tube) are simulation input parameters; μ_a(fit) and μ_s'(fit) are obtained by fitting diffusion theory to the simulation data; and μ_a(cal) is calculated from Eq. (7). Other common parameters used for four cases in the table are α=0.5, β=1, μ_a(back)=0.05 cm^{-1}, and μ_s'(back)=μ_s'(tube)=10 cm^{-1}. We can see that the ratio of μ_a(fit)/μ_a(cal) under various conditions is very close to 1, indicating the consistency between Eq. (7) and the simulations.

VI. DISCUSSION

The findings from the experiments of the tissue phantoms and the Monte Carlo simulations suggest that Eq. (7) is an adequate description of the dependence of μ_a(sys) on μ_a(back) and μ_a(tube). This relationship is nonlinear and leads to a complicated analysis of reflectance data from composite biological tissues. However, the experimental results given in Sec. III display a linear range between μ_a(sys) and μ_a(tube), and this range varies, depending on tube diameters and values of the μ_a(tube). In this section, we first study general characteristics of Eq. (7), and investigate the criteria in which Eq. (7) gives a linear dependence of μ_a(sys) on the μ_a(tube). Then the focus shifts to whether the linear relationship still holds in blood–tissue systems. Finally, combining the developed formula with *in vivo* measurement results, we discuss improved algorithms for blood oxygenation determination in biological tissues.

A. Nonlinearity of Eq. (7)

The nonlinear dependence of μ_a(sys) on the tube diameter, d, and μ_a(tube) is introduced by the exponential term in Eq. (7). It follows that larger tube diameters in the resin-tube system give rise to larger values of "m," and thus to smaller

TABLE II. Comparison of absorption coefficients obtained from the Monte Carlo simulations and from Eq. (7) for the resin-tube model.

d (cm)	r_t [%]	μ_a (tube) (cm^{-1})	μ_a (fit) (cm^{-1})	μ_a (cal)[a] (cm^{-1})	$\frac{\mu_a(\text{fit})}{\mu_a(\text{cal})}$	$\frac{\mu_s'(\text{fit})}{\mu_s'(\text{tube})}$ [b]
0.4	34.9	0.5	0.205	0.194	1.06	1.01
0.4	34.9	2.5	0.666	0.669	1.00	0.98
0.2	8.73	2.5	0.231	0.217	1.06	0.94
0.2	8.73	3.5	0.238	0.263	0.90	0.99

[a] α=0.5, β1=1, μ_a(back)=0.05 cm^{-1}.
[b] μ_s'(tube)=μ_s'(back)=10 cm^{-1}.

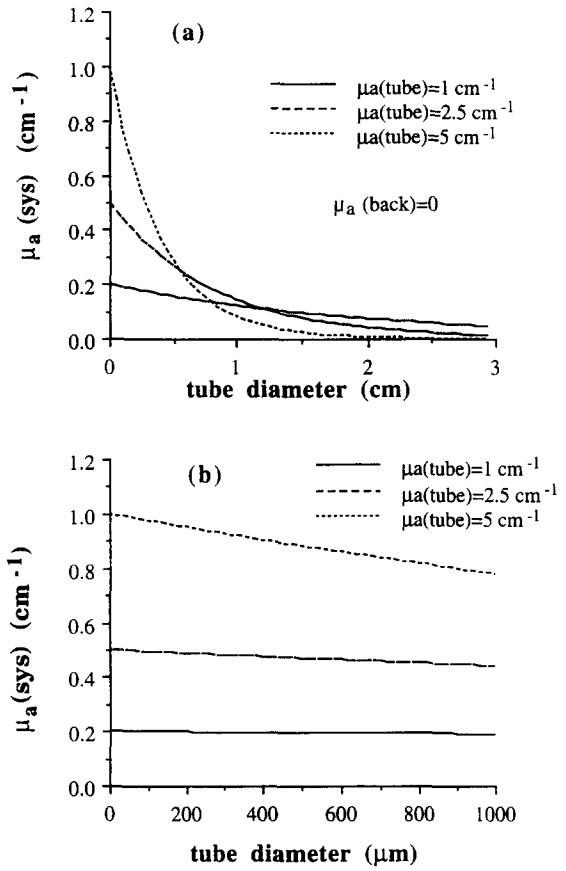

FIG. 7. Dependence of μ_a(sys) on large tube diameters (a) and small tube diameters (b) of the distributed absorbers. The tube-to-sample volume ratio is 20%, and the values of μ_a(tube) are 1 cm^{-1} (solid line), 2.5 cm^{-1} (dashed line), and 5 cm^{-1} (dotted line).

values of μ_a(sys), while keeping other conditions the same. Figure 7(a) shows the dependence of μ_a(sys) on the tube diameter for three different μ_a(tube) values and the same volume ratio of 20%. It is clear that μ_a(sys) is smaller for larger values of d. This means that in a system consisting of small- and large-diameter vessels, the detected photons more likely come through small vessels than through large vessels. The photons entering a large vessel are more likely to be absorbed before they leave the vessel than they are in a small vessel. However, as Fig. 7(b) demonstrates, μ_a(sys) is approximately independent of the tube diameter when tube diameters are less than 1 mm, particularly if the absorption in the tubes is not too high, such as μ_a(tube)=1 and 2.5 cm^{-1}. So small vessels with diameters thinner than a few hundred micrometers contribute much more to the detected signal than do large vessels.

B. Linearization of Eq. (7)

After substituting $\alpha=0.5$ and $\beta=1$ in Eq. (7), we have

$$\mu_a(\text{sys})=\mu_a(\text{back})+r_t e^{-0.5d[\mu_a(\text{tube})-\mu_a(\text{back})]}[\mu_a(\text{tube})-\mu_a(\text{back})]. \quad (9)$$

Expanding the exponential term to the first order yields

$$\mu_a(\text{sys})=\mu_a(\text{back})+r_t\{1-0.5d[\mu_a(\text{tube})-\mu_a(\text{back})]\}\times[\mu_a(\text{tube})-\mu_a(\text{back})]. \quad (10)$$

When

$$0.5d[\mu_a(\text{tube})-\mu_a(\text{back})]\ll 1, \quad (11)$$

we obtain a linear equation between μ_a(sys) and μ_a(tube):

$$\mu_a(\text{sys})=(1-r_t)\mu_a(\text{back})+r_t\mu_a(\text{tube}). \quad (12)$$

This equation states that in a two-component system, the apparent absorption coefficient equals a sum of the absorption coefficients of the components weighted by the component volume fraction. Equation (11) indicates that the linear approximation is justified when either the tube diameter, d, or the absorption difference between the background and the solution in the tubes is small. This explains why the sample with smaller diameter tubes has a larger linear range than the sample with larger diameter tubes, as shown in Fig. 3. We can estimate a threshold value of $\mu_a(\text{tube})_{\text{th}}$, below which μ_a(sys) and μ_a(tube) are linearly related, by replacing Eq. (11)

$$0.5d[\mu_a(\text{tube})_{\text{th}}-\mu_a(\text{back})]\leq 0.1. \quad (13)$$

Thus, we obtain $\mu_a(\text{tube})_{\text{th}}$ values of 0.3, 0.6, and 1.25 cm^{-1} for the resin-tube samples with 6.4, 3.2, and 1.6 mm diam, respectively. These data are in agreement with the μ_a(tube) values, below which μ_a(sys) is linearly dependent on μ_a(tube), as observed in Figs. 2 and 3.

C. Blood–tissue systems

In the case of blood oxygenation determined by time-resolved reflectance measurements, it is useful to know whether the linear relationship given in Eq. (12) can be applied to blood–tissue systems.

The absorption coefficient of whole blood at $\lambda=780$ nm can be estimated by

$$\mu_a(\text{blood})^{780}=[c]\epsilon^{780}=8\ \text{mM}\times 0.46\ \text{cm}^{-1}\,\text{mM}^{-1}=3.68\ \text{cm}^{-1},$$

where $[c]=8$ mM is the blood hemoglobin concentration, and $\epsilon^{780}=0.46$ cm^{-1} mM^{-1} takes an average value of extinction coefficients of oxygenated and deoxygenated hemoglobin at 780 nm.[25] Depending on the oxygenation status of the blood, values of μ_a(blood) are 3–5 cm^{-1} in the near-infrared range. The background absorption is, in general, much lower than blood absorption. For example, we found that μ_a(back) is 0.06 cm^{-1} for blood-free brain tissues. According to Eq. (13), if the blood vessels have diameters equal to or smaller than $0.2/(3.00-0.06)\approx 0.07$ cm=700 μm, Eq. (12) is then valid, and μ_a(sys) depends linearly on μ_a(blood). Most blood vessels in tissue have diameters smaller than 700 μm. Thus, we suggest that the apparent absorption coefficient, μ_a(sys), of a blood-filled biological organ can be approximated by a volume-weighted sum of absorption coefficients of whole blood and background tissue.

Furthermore, Eq. (12) results in

$$\Delta\mu_a(\text{sys})\cong r_t\,\Delta\mu_a(\text{blood}), \quad (14)$$

TABLE III. List of absorption coefficients measured *in vivo* with or without blood on animal and human heads and on rat liver by a time-resolved reflectance at 780 nm. $\Delta\mu_a^{780}(\text{blood})=3.68\ \text{cm}^{-1}$.

	Dog head	Piglet head	Rat liver[22]	Human head
Separation ρ (cm)	3	3	1.8–2	3
μ_a^{780}(sys) (cm^{-1})	0.16±0.01	0.18±0.01	1.08[a]	0.15±0.01
μ_a^{780}(back) (cm^{-1})	0.08±0.005	0.10±0.007	0.42±0.01	
$\Delta\mu_a^{780}$(sys) (cm^{-1})	0.08±0.01	0.08±0.01	0.66	
r_t [%]	2.2	2.2	18	

[a]Refer to Ref. 22 for the estimation of this high μ_a value.

and gives a means to study the response of μ_a(sys) to the change of μ_a(blood) in vessels. Table III lists some apparent absorption coefficients measured *in vivo* in animals and humans, with the time-resolved technique at 780 nm. In this table, μ_a^{780}(sys) represents the results under normal conditions for both animals and humans, whereas μ_a^{780}(back) corresponds to the blood-free absorption measured only in animals. The value of $\Delta\mu_a^{780}$(sys) is equal to $\mu_a^{780}(\text{sys})-\mu_a^{780}(\text{back})$, and $\Delta\mu_a^{780}$(blood) is calculated, based on $\Delta\mu_a^{\lambda}=\Delta[c]\Delta\epsilon^{\lambda}$. For the change from a normal to blood-free condition, we assume $\Delta[c]=8$ mM and $\Delta\epsilon^{780}=0.46\ \text{cm}^{-1}\,\text{mM}^{-1}$. These two values lead to $\Delta\mu_a^{780}(\text{blood})=3.68\ \text{cm}^{-1}$. Thus, Eq. (14) gives rise to a vessel-to-organ volume ratio, r_t for the head and liver in animals. The calculated blood-to-brain volume ratio of 2.2% seems a little too small for animal heads. Several possible explanations for underestimating the ratio are (i) although the actual blood-to-brain volume ratio[26,27] may be about 5%, the optical field of the near-infrared light includes the skin and skull and a part of the brain. The inclusion of the skull makes the blood-to-sample volume ratio decrease; (ii) some leftover blood in vessels increases the background absorption, μ_a^{780}(back), and thus decreases the value of $\Delta\mu_a^{780}$(sys); and (iii) variation of blood concentration, $[c]$, and extinction coefficient for different saturation states may cause a deviation of $\Delta\mu_a^{780}$(blood) from the theoretical value of 3.68 cm^{-1}. In spite of smaller values of r_t for the animal brain results, the *in vivo* data given in Table III are in reasonable agreement with Eq. (14).

D. Determination of hemoglobin oxygenation

The purpose of having an accurate μ_a(sys) at wavelength λ is to determine hemoglobin oxygenation noninvasively. The widely used two-wavelength algorithm is based on the assumption that the oxygenated and deoxygenated hemoglobin are the only two components absorbing the near-infrared light. This leads to

$$\mu_a^{\lambda 1}=[\text{Hb}]\epsilon_{\text{Hb}}^{\lambda 1}+[\text{HbO}_2]\epsilon_{\text{HbO}_2}^{\lambda 1} \tag{15a}$$

$$\mu_a^{\lambda 2}=[\text{Hb}]\epsilon_{\text{Hb}}^{\lambda 2}+[\text{HbO}_2]\epsilon_{\text{HbO}_2}^{\lambda 2}, \tag{15b}$$

where [Hb] and [HbO_2] are deoxygenated and oxygenated, respectively, hemoglobin concentrations in blood, and $\epsilon_{\text{Hb}}^{\lambda}$ and $\epsilon_{\text{HbO}_2}^{\lambda}$ are extinction coefficients at wavelength λ, and can be found in previously published studies.[25] The hemoglobin saturation, Y, is defined as $Y=[\text{HbO}_2]/\{[\text{HbO}_2]+[\text{Hb}]\}$ and can be solved from Eqs. (15a) and (15b) as

$$Y=\frac{a\epsilon_{\text{Hb}}^{\lambda 2}-\epsilon_{\text{Hb}}^{\lambda 1}}{(\epsilon_{\text{HbO}_2}^{\lambda 1}-\epsilon_{\text{Hb}}^{\lambda 1})-a(\epsilon_{\text{HbO}_2}^{\lambda 2}-\epsilon_{\text{Hb}}^{\lambda 2})}, \tag{16}$$

where $a=\mu_a^{\lambda 1}/\mu_a^{\lambda 2}$ can be measured from the time- or frequency-domain techniques.[4] From our study, it is clear that the measured μ_a^{λ} is a volume-weighted sum of the absorption as a result of both the whole blood in vessels and the background tissue. Although the value of μ_a(tissue) is, in general, much smaller than the value of μ_a(blood), the contribution of μ_a(tissue) to μ_a(sys) cannot be neglected because the volume ratio for the background tissue is rather large. Table III shows unambiguously that in many cases the background absorption contributes to the signal as much as does the blood.

To consider background tissue, we use Eq. (12), and have

$$\mu_a^{\lambda 1}=r_{\text{blood}}([\text{Hb}]\epsilon_{\text{Hb}}^{\lambda 1}+[\text{HbO}_2]\epsilon_{\text{HbO}_2}^{\lambda 1})+\delta^{\lambda 1}, \tag{17a}$$

$$\mu_a^{\lambda 2}=r_{\text{blood}}([\text{Hb}]\epsilon_{\text{Hb}}^{\lambda 2}+[\text{HbO}_2]\epsilon_{\text{HbO}_2}^{\lambda 2})+\delta^{\lambda 2}, \tag{17b}$$

where r_{blood} is the volume ratio occupied by blood vessels, $\delta^{\lambda 1}=(1-r_{\text{blood}})\mu_a^{\lambda 1}$(tissue), and $\delta^{\lambda 2}=(1-r_{\text{blood}})\mu_a^{\lambda 2}$(tissue). However, parameters of r_{blood} and $\mu_a^{\lambda 1}$(tissue) are often not available in the clinical environment. To solve this problem, we assume the absorption of background tissue, δ(tissue) or μ_a(tissue) to be wavelength independent, since the absorption band of hemoglobin-free tissue should be quite flat in the near-infrared range. Based on this assumption, we suggest several possible solutions to calculate hemoglobin oxygenation. One solution is that absorption coefficients of blood-free samples, δ(tissue), for various kinds of tissues are premeasured in laboratories and entered into an empirical table. Then accurate hemoglobin saturation values can be obtained based on the two-wavelength formula, Eq. (16), just by replacing $\mu_a^{\lambda 1}/\mu_a^{\lambda 2}$ with $[\mu_a^{\lambda 1}(\text{sys})-\delta]/[\mu_a^{\lambda 2}(\text{sys})-\delta]$. A second solution, on the other hand, adds a third wavelength as an extra equation to Eqs. (17a) and (17b), and these three enable us to solve for r_{blood}[Hb], r_{blood}[HbO_2], and δ. The expression for hemoglobin saturation, Y, is then obtained as

$$Y=\frac{(a-1)\epsilon_{\text{Hb}}^{\lambda 3}-(a-c)\epsilon_{\text{Hb}}^{\lambda 2}-(c-1)\epsilon_{\text{Hb}}^{\lambda 1}}{-(a-1)\epsilon_{\Delta\ \text{Hb}}^{\lambda 3}+(a-c)\epsilon_{\Delta\ \text{Hb}}^{\lambda 2}+(c-1)\epsilon_{\Delta\ \text{Hb}}^{\lambda 1}}, \tag{18}$$

where $a=\mu_a^{\lambda 1}/\mu_a^{\lambda 2}$, $c=\mu_a^{\lambda 3}/\mu_a^{\lambda 2}$, and $\epsilon_{\Delta\ \text{Hb}}^{\lambda}=\epsilon_{\text{HbO}_2}^{\lambda}-\epsilon_{\text{Hb}}^{\lambda}$. Quantities of "$a$" and "$c$" are determined from measurements.

Figure 8 shows a comparison of simulated results for a hemoglobin oxygenation calculation using three algorithms: a two-wavelength method without background subtraction, a two-wavelength method with background subtraction, and a three-wavelength method. Parameters used for this figure are $\lambda_1=780$ nm, $\lambda_2=830$ nm, $\lambda_3=750$ nm, $r_t=5\%$, $[\text{Hb}]+[\text{HbO}_2]=8$ mM, $\delta=0.95\mu_a^{\lambda}$(tissue), and $\mu_a^{750\text{-}830}(\text{tissue})=0.05\ \text{cm}^{-1}$. It is clear that the two-wavelength algorithm without the background subtraction has errors as much as 20%, particularly near the 100% oxy-

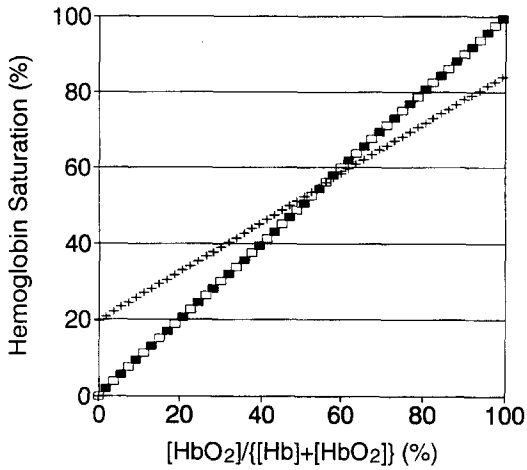

FIG. 8. A comparison of simulated results of hemoglobin oxygenation calculated using a two-wavelength method without the background subtraction (plus sign), a two-wavelength method after the background subtraction (solid squares), and a three-wavelength method (open squares).

genated and deoxygenated ranges. In contrast, either the three-wavelength method or the two-wavelength method with the background correction gives more accurate results. However, further investigations, particularly for *in vivo* measurements, are needed to determine whether it is suitable to assume δ to be wavelength independent.

E. Summary

In this paper, we first investigated a heterogeneous tissue-vessel model experimentally using time-resolved reflectance. Specifically, we studied the dependence of the apparent absorption coefficient μ_a(sys) on tube distribution, tube sizes, and the absorption inside the tubes. The results show that the accurate relationship between μ_a(sys) and μ_a(tube) is nonlinear, proportional to the absorbers' volume ratio, and has an exponential decay term. The Monte Carlo simulation verified these findings. This complex relationship between μ_a(sys) and μ_a(tube), however, becomes a simple volume-weighted sum of the absorption coefficients of different absorbing components for biological samples when blood-vessel diameters are smaller than a few hundred micrometers. The results *in vivo* support the findings. Furthermore, we suggest two improved algorithms to correct tissue background absorption for accurate hemoglobin oxygenation determination.

ACKNOWLEDGMENTS

The authors wish to thank C. Dean Kurth, University of Pennsylvania and Children's Hospital of Philadelphia, for sharing the animal *in vivo* results, and to Lihong Wang, M. D. Anderson Cancer Center, The University of Texas at Houston, for his assistance on the time-resolved Monte Carlo simulations.

[a]Also at Rice University.

[1]F. F. Jöbsis, "Noninvasive, infrared monitoring of cerebral and myocardial oxygen sufficiency and circulatory parameters," Science **19**, 1264 (1977).

[2]M. Ferrari, E. Zanetti, I. Giannini, G. Sideri, C. Fieschi, and A. Carpi, "Effects of carotid artery compression test on regional cerebral blood volume, haemoglobin oxygen saturation and cytochrome-c-oxidase redox level in cerebrovascular patients," Adv. Exp. Med. Biol. **200**, 213–222 (1986).

[3]B. Chance, S. Nioka, J. Kent, K. McCully, M. Fountain, R. Greenfeld, and G. Holtom, "Time-resolved spectroscopy of hemoglobin and myoglobin in resting and ischemic muscle," Anal. Biochem. **174**, 698–707 (1988).

[4]E. M. Sevick, B. Chance, J. Leigh, S. Nioka, and M. Maris, "Quantitation of time- and frequency-resolved optical spectra for the determination of tissue oxygenation," Anal. Biochem. **195**, 330–351 (1991).

[5]D. A. Benaron, W. E. Benitz, R. L. Ariagno, and D. K. Stevenson, "Noninvasive methods for estimating in vivo oxygenation," Clin. Pediatr. **31**, 258 (1992).

[6]C. E. Elwell, M. Cope, A. D. Edwards, J. S. Wyatt, and E. O. R. Reynolds, "Measurement of cerebral blood flow in adult humans using near infrared spectroscopy: Methodology and possible errors," Adv. Exp. Med. Biol. **317**, 235–245 (1992).

[7]D. S. Smith, W. J. Levy, S. Carter, N. Wang, M. Haida, and B. Chance, "Time resolved spectroscopy and the determination of photon scattering, pathlength and brain vascular hemoglobin saturation in a population of normal volunteers," Proc. SPIE Int. Soc. Opt. Eng. **1888**, 511–515 (1993).

[8]S. J. Matcher and C. E. Cooper, "Absolute quantification of deoxyhaemoglobin concentration in tissue near infrared spectroscopy," Phys. Med. Biol. **39**, 1–17 (1994).

[9]B. C. Wilson, "Optical properties of tissues," in *Encyclopedia of Human Biology*, (Academic, New York, 1991), Vol. 5, p. 587.

[10]S. Wray, M. Cope, D. T. Delpy, J. S. Wyatt, and E. Reynolds, "Characterization of the near infrared absorption spectra of cytochrome aa3 and haemoglobin for the non-invasive monitoring of cerebral oxygenation," Biochim. Biophys. Acta **933**, 184 (1988).

[11]A. H. Hielscher, F. K. Tittel, and S. L. Jacques, "Noninvasive monitoring of blood oxygenation by phase resolved transmission spectroscopy," Proc. SPIE Int. Soc. Opt. Eng. **1888**, 275–288 (1993).

[12]M. Cope and D. T. Delpy, "System for long-term measurement of cerebral blood and tissue oxygenation on newborn infants by near infrared transillumination," Med. Biol. Eng. Comput. **26**, 289 (1988).

[13]B. Chance, J. S. Leigh, H. Miyaka, D. S. Smith, D. S. Niola, R. Greenfeld, M. Finander, K. Kaufmann, W. Levy, M. Young, P. Cchen, P. Yoshioka, and R. Boretsky, "Comparison of time resolved and unresolved measurements of deoxyhemoglobin in brain," Proc. Natl. Acad. Sci. **85**, 4971 (1988).

[14]M. Thorniley, L. Livera, Y. Wickramasinghe, S. A. Spencer, and P. Rolfe, "The noninvasive monitoring of cerebral tissue oxygenation," Adv. Exp. Med. Biol. **277**, 323 (1990).

[15]T. Tamura, H. Eda, M. Takada, and T. Kubodera, "New instrument for monitoring hemoglobin oxygenation," Adv. Exp. Med. Biol. **248**, 103–107 (1990).

[16]M. Firbank, M. Hiraoka, and D. T. Delpy, "Development of a stable and reproducible tissue equivalent phantom for use in infrared spectroscopy and imaging," Proc. SPIE Int. Soc. Opt. Eng. **1888**, 264–274 (1993).

[17]D. V. O'Connor and D. Phillips, *Time-Correlated Single Photon Counting* (Academic, Orlando, FL, 1984).

[18]H. Liu, M. Miwa, B. Beauvoit, N. G. Wang, and B. Chance, "Characterization of absorption and scattering properties of small-volume biological samples using time-resolved spectroscopy," Anal. Biochem. **213**, 378–385 (1993).

[19]M. S. Patterson, B. Chance, and B. C. Wilson, "Time resolved reflectance and transmittance for the non-invasive measurement of tissue optical properties," Appl. Opt. **28**, 2331–2336 (1989).

[20]A. H. Hielscher, L. Wang, F. K. Tittel, and S. L. Jacques, "Influence of boundary conditions on the accuracy of diffusion theory in time-resolved reflectance spectroscopy of biological tissues," accepted for publication in Phys. Med. Biol.

[21]C. D. Kurth, H. Liu, W. Thayer, and B. Chance, "Dynamic phantom brain model for near-infrared spectroscopy," Phys. Med. Biol. (to be published).

[22]T. Kitai, B. Beauvoit, H. Liu, and B. Chance, "Changes in the light path length of blood perfused rat liver by increased hematocrit and anoxia," Proc. SPIE Int. Soc. Opt. Eng. **2326**, 326–333 (1994).

[23]P. Horowitz and W. Hill, *The Art of Electronics* (Cambridge U.P., Cambridge, 1988), pp. 625–626.

[24]L. Wang and S. L. Jacques, *Monte Carlo Modeling of Light Transport in Multi-Layered Tissues in Standard C*, Laser Biology Research Laboratory, The University of Texas, M. D. Anderson Cancer Center, Houston, TX.

[25]W. G. Zijlstra, A. Buursma, and W. P. Meeuwsen-van der Roest, "Absorption spectra of human fetal and adult oxyhemoglobin, deoxyhemoglobin, carboxyhemoglobin, and Met hemoglobin," Clin. Chem. **37**, 1633–1638 (1991).

[26]R. L. Grubb, Jr., M. E. Raichle, J. O. Eichling, and M. M. Ter-Pogossian, "The effects of changes in $PaCO_2$ on cerebral blood volume, blood flow, and vascular mean transit time," Stroke **5**, 630–639 (1974).

[27]M. M. Todd, J. B. Weeks, and D. S. Warner, "The influence of intravascular volume expansion on cerebral blood flow and blood volume in normal rats," Anesthesiology **78**, 945–953 (1993).